2024 European Control Conference (ECC)
June 25-28, 2024. Stockholm, Sweden

Enhancing Resilience in Angle Droop Control of Inverter-interfaced Microgrids

Mahdieh S. Sadabadi[1] and Xiaodong Cheng[2]

Abstract— **This paper develops a resilient angle control strategy for inverter-interfaced microgrids subject to magnitude-bounded disturbance. We show that an inverter-interfaced microgrid can be cast as a Lur'e system (a combination of a linear time-invariant system and a nonlinear static state feedback sector-bounded nonlinearity). Then, under this novel description and use of mathematically rigorous input–output stability analysis results, the stability of inverter-based microgrids will be analyzed. The resilience analysis of the microgrids controlled by the proposed angle control approach is based on a mathematically rigorous characterization of disturbances that a microgrid can tolerate so that its stability and operational constraints are not violated. The simulation results evaluate the performance and effectiveness of the proposed resilient angle control over conventional angle droop control methods.**

I. Introduction

Microgrids are defined by IEC 62898-1:2017 [1] as a group of interconnected loads and distributed energy resources with defined electrical boundaries, which act as a single controllable entity and operate in both grid-connected and island mode. The high integration of renewable energy and inverter-based resources in microgrids poses new challenges for modernized power generation due to the low inertia characteristics of such systems. The challenges are in terms of stability issues and reducing the system's resilience in response to disturbances [2]–[4]. The South Australian blackout of 2016 was the first known blackout due to high renewable penetration with low system inertia [5]. According to the Australian Energy Market Operator (AEMO) [6], the technical reason for the 2016 blackout was the sudden voltage angle changes and rapid load variations. The South Australian blackout event highlights the importance of voltage phase angles in the stability of invert-based power generation and the resilient design of control schemes for inverters.

Angle droop control is one of the well-known control approaches introduced in [7], which was motivated by the fact that small voltage angle differences among inverter-based resources (IBRs) cause a change in the power-sharing between the resources. An angle droop-controlled inverter measures its active power to regulate its phase angle [8]. Certain design criteria ensure proportional active power sharing among IBRs [8]. Although the implementation of an angle droop control strategy is harder than frequency droop control, it provides several advantages over frequency droop control methods including improved stability margins and transient response as well as frequency synchronization [9].

Various types of angle droop control techniques have been proposed in the literature, e.g., [8], [10], [11] and references therein. A distributed control scheme for improving the stability margin and ensuring the desired power sharing in angle droop-controlled microgrids was proposed in [8]. An inverse optimal control framework for angle stabilization in an inverter-based generation was presented in [11].

Due to the higher penetration of renewable energy resources and distributed generators in inverter-based microgrids, the occurrence of disturbance has significantly increased [12]. The sources of typical disturbance in these systems include load shedding, generation tripping, intermittent power outputs of renewable-based generation units, and cyber-attacks. Therefore, it is required to develop novel methods for the resilience analysis of inverter-based systems and quantify the critical disturbance levels that an inverter-based microgrid can withstand and propose resilient control frameworks to enhance the normal operation of these systems in the presence of disturbances. The common resilience analysis methods based on $\mathscr{H}_2$ and $\mathscr{H}_\infty$ norms cannot be suitable for analyzing the resilience of inverter-based microgrids and measuring the maximum magnitude of disturbances applied to these systems while transient stability and operational constraints such as frequency constraints are satisfied. The main reason is that $\mathscr{H}_2$ and $\mathscr{H}_\infty$ norms evaluate the energy of outputs rather than the magnitude of output signals [13]. Moreover, although the existing angle control methods deal with frequency synchronization and power-sharing objectives in inverter-based power networks, the transient stability and resilience behavior of these systems against disturbances have not been considered. Hence, it is required to modify the existing droop control strategies by enforcing a resilient feature in their design process.

This paper aims to develop a novel angle droop control strategy with built-in resilient solutions to enhance the resilience and optimal operation of inverter-interfaced microgrids while under disturbances. To this end, the inverter-based generation system is represented by a Lur'e system, which is a combination of a linear time-invariant system and a nonlinear static state feedback sector-bounded nonlinearity. By virtue of this novel representation, the inverter-based microgrid is seen as an input–output map from the disturbance to the phase angle deviation of IBRs. Using input-output stability analysis results for Lur'e systems, the stability and resilient feature of angle droop-controlled inverter-based mi-

[1] M. S. Sadabadi is with the Department of Electrical and Electronic Engineering, The University of Manchester, Manchester, United Kingdom (mahdieh.sadabadi@manchester.ac.uk)

[2] X. Cheng is with Mathematical and Statistical Methods - Biometris, Wageningen University & Research, 6708 PB Wageningen, The Netherlands (xiaodong.cheng@wur.nl)

crogrids will be analyzed. Using a mathematically rigorous resilience analysis framework based on $\mathscr{L}_\infty$ norms of systems [14], we show that the proposed resilient angle droop control can withstand large disturbances (in terms of the magnitude of disturbances) compared to the conventional angle droop control methods without violating the frequency constraints. Simulation results and comparative case studies are presented to evaluate the performance and effectiveness of the proposed angle droop control approach.

The paper is organized as follows. The problem statement is presented in Section II. Section III proposes the resilient angle droop control strategy. Section IV is devoted to the input-state stability analysis. Simulation results are presented in Section V. Finally, Section VI concludes this paper.

Notation. The notation used in this paper is standard. In particular, $\mathbf{1}_n$, $\mathbf{0}_n$, $\mathbf{I}_n$, and $\mathbf{0}_{n\times m}$ are an $n\times 1$ vector of ones, an $n\times 1$ zero vector, an $n\times n$ Identity matrix, and a zero matrix of dimension $n\times m$, respectively. For an $n\times m$ matrix A, $\rho(A)$ is the symbol of the spectral radius of A and $(A)^{|.|}$ is a matrix of size $n\times m$ whose elements are the absolute value of the elements of A.

Preliminary. For an $n\times n$ positive matrix $A\geq 0$, $M=\mathbf{I}_n-A$ is inverse-positive if M^{-1} exists and $M^{-1}\geq 0$, or equivalently $\rho(A)<1$ [15]. For a vector $x\in\mathbb{R}^n$, the element-wise $\mathscr{L}_\infty$ norm is denoted by $\|x\|_{\mathscr{L}_\infty}\in\mathbb{R}^n$ whose i-element is obtained as follows:

$$[\|x\|_{\mathscr{L}_\infty}]_i=\sup_{t\geq 0}|x_i(t)|.$$

For a stable LTI system with a bounded $\mathscr{L}_\infty$-norm input $u\in\mathbb{R}^m$ and output $y\in\mathbb{R}^n$ represented by a transfer function matrix $G(s)$, the following inequality is satisfied [12]

$$\|y\|_{\mathscr{L}_\infty}\leq\gamma_G\|u\|_{\mathscr{L}_\infty}$$

where $\gamma_G\in\mathbb{R}^{n\times m}$ the gain matrix is defined as the gain matrix and its ij element is obtained as follows [12]:

$$\gamma_{G,ij}=\int_{-\infty}^{\infty}|g_{ij}(\tau)|d\tau, \tag{1}$$

where g_{ij} is the impulse response of $G_{ij}(s)$.

II. Problem Statement

Consider a lossless Kron-reduced network consisting of n IBRs interconnected via inductive power lines. Each IBR i, $i=1,\ldots,n$, is represented by a voltage phasor modeled by a constant magnitude (1 per unit) and controllable angle dynamics $\theta_i(t)$. The IBR dynamics are presented as follows:

$$\dot{\theta}(t)=u(t)+\omega^*\mathbf{1}_n, \tag{2}$$

where $\theta(t)=[\theta_1(t),\ldots,\theta_n(t)]^T\in\mathbb{R}^n$ is the vector of phase angles of inverters, $u(t)=[u_1(t),\ldots,u_n(t)]^T\in\mathbb{R}^n$ is the control input vector, and $\omega^*\in\mathbb{R}$ is a reference frequency.

The underlying network can be presented by a weighted directed graph $\mathbb{G}=(\mathbb{V},\Xi,\mathbb{E})$. Each element in the vertex set $\mathbb{V}$, $|\mathbb{V}|=n$, and the edge set $\mathbb{E}$, $|\mathbb{E}|=m$ respectively represent an IBR and an inductive power line with susceptance $b_{ij}>0$, $(i,j)\in\mathbb{E}$. The weighting matrix Ξ is defined as $\Xi=\text{diag}(b_{ij})$, $(i,j)\in\mathbb{E}$. The topology of the graph $\mathbb{G}$ is described by an incidence matrix $\mathbb{B}\in\mathbb{R}^{n\times m}$ and the weighted Laplacian matrix of the underlying graph is $\mathbb{L}=\mathbb{B}\Xi\mathbb{B}^T$.

Let us define $\theta^*(t)=\omega^*\mathbf{1}_n t+\theta_0^*\in\mathbb{R}^n$ and $\theta_0^*=[\theta_{1,0}^*,\ldots,\theta_{n,0}^*]^T\in\mathbb{R}^n$ as the reference and initial angle vector, respectively. The main objective is to design $u(t)$ so that the frequency synchronization is achieved at the steady-state, i.e.,

$$lim_{t\to\infty}\omega(t)=\omega^*. \tag{3}$$

Assumption 1: The initial reference angle vector θ_0^* satisfies $\mathbb{B}^T\theta_0^*\in(-\frac{\pi}{2},\frac{\pi}{2})^m$.

Assumption 1, commonly referred to as a *security constraint* [16], implies that the absolute values of the difference in the reference voltage phase angles between neighboring IBRs are not larger than $\frac{\pi}{2}$.

The deviation of the active electrical power $P_{e,i}\in\mathbb{R}$ injected into the network at IBR i and the nominal power $P_{e,i}^*\in\mathbb{R}$ drawn from the dc source of IBR i is given as [11]:

$$P_{e,i}(\theta)-P_{e,i}^*(\theta^*)=\sum_{j\in\mathscr{N}_i}|V_i||V_j|b_{ij}\left(sin(\theta_{ij})-sin(\theta_{ij}^*)\right), \tag{4}$$

where $\theta_{ij}=\theta_i-\theta_j$, $\theta_{ij}^*=\theta_i^*-\theta_j^*$, $|V_i|$ is the nodal voltage magnitude of IBR i, $\mathscr{N}_i$ is the set of neighbors of the i-th IBR, and b_{ij} is the susceptance of the line connecting IBRs i and j. The voltage magnitudes $|V_i|$ at are regulated by internal controllers to constant values, i.e., $|V_i|=1$ per unit. To achieve the frequency synchronization in (3), [11] proposes the following angle droop controller for the i-th IBR, which is based on an inverse optimal control strategy:

$$u_i(t)=-\frac{1}{2r_i}\left(\theta_i(t)-\theta_i^*(t)+m_{\theta_i}(P_{e,i}(\theta)-P_{e,i}^*(\theta^*))\right) \tag{5}$$

where $r_i>0$ is a positive gain and $m_{\theta_i}>0$ is the $P-\theta$ droop gain. The proposed angle controller in (5) stabilizes the phase angle vector with respect to a nominal steady-state angle and ensures frequency synchronization at stationery. Moreover, (5) can have inherent robustness properties against additive disturbances, as the solution to an optimal control problem with the suitable choice of a cost function [11]. However, it is not inherently resilient to any manipulation of sensors, control inputs, and communication links, in the sense that it cannot guarantee that transient stability and operational constraints such as frequency constraints are satisfied under disturbances. The main objective of this paper is to design a resilient-by-design angle control scheme for inverter-interfaced microgrids by modifying (5) to enhance their resilience against external disturbances.

III. Proposed Resilient Angle Control Strategy

The main goal is to use angle measurements from phasor measurement units (PMUs) and synthesize a controller that enhances the resilience of (5) against disturbance signals while achieving angle stabilization and frequency synchronization in inverter-interfaced microgrids. The proposed an-

gle control law for IBR i, $i=1,\ldots,n$, is presented as follows:

$$\begin{aligned} u_i(t) &= -\frac{1}{2r_i}\left(\theta_i(t)-\theta_i^*(t)+m_{\theta_i}(P_{e,i}(\theta)-P_{e,i}^*(\theta^*))\right) \\ &\quad -\beta_i x_{c_i}(t), \\ \dot{x}_{c_i}(t) &= \beta_i\left(\theta_i(t)-\theta_i^*(t)+m_{\theta_i}(P_{e,i}(\theta)-P_{e,i}^*(\theta^*))\right) \\ &\quad -\eta_i x_{c_i}(t), \end{aligned} \tag{6}$$

where $\eta_i>0$, $\beta_i\geq 0$ are scalars and $x_{c_i}(t)\in\mathbb{R}$ is an auxiliary control state. Note that if the value of β_i, $i=1,\ldots,n$, is selected to be zero, the proposed controller in (6) is the same as the one in (5). The dynamics of the inverter-interfaced power generation system with the proposed control strategy in (6) can be written as follows:

$$\begin{aligned} \dot{\theta}_i(t) =& \frac{-1}{2r_i}\left((\theta_i(t)-\theta_i^*(t))+m_{\theta_i}\sum_{j\in\mathscr{N}_i} b_{ij}\left(\sin(\theta_{ij}(t))-\sin(\theta_{ij}^*)\right)\right) \\ & -\beta_i x_{c_i}(t)+\omega^*, \\ \dot{x}_{c_i}(t) =& \beta_i\left((\theta_i(t)-\theta_i^*(t))+m_{\theta_i}\sum_{j\in\mathscr{N}_i} b_{ij}\left(\sin(\theta_{ij}(t))-\sin(\theta_{ij}^*)\right)\right) \\ & -\eta_i x_{c_i}(t). \end{aligned} \tag{7}$$

Let us assume that $\bar{\theta}_i=\lim_{t\to\infty}\theta_i(t)$ be an induced steady-state angle of the i-th IBR. Moreover, $\bar{x}_{c_i}=\lim_{t\to\infty}x_{c_i}(t)$. By change of variables as $\tilde{\theta}_i=\theta_i-\theta_i^*$, the dynamics of the inverter-based system with the proposed control strategy in (6) can be written as follows:

$$\begin{aligned} \dot{\tilde{\theta}}_i(t) =& -\frac{1}{2r_i}\left(\tilde{\theta}_i(t)+m_{\theta_i}\sum_{j\in\mathscr{N}_i} b_{ij}\left(\sin(\tilde{\theta}_{ij}(t)+\theta_{ij}^*)-\sin(\theta_{ij}^*(t))\right)\right) \\ & -\beta_i x_{c_i}(t), \\ \dot{x}_{c_i}(t) =& \beta_i\left(\tilde{\theta}_i(t)+m_{\theta_i}\sum_{j\in\mathscr{N}_i} b_{ij}\left(\sin(\tilde{\theta}_{ij}(t)+\theta_{ij}^*(t))-\sin(\theta_{ij}^*)\right)\right) \\ & -\eta_i x_{c_i}(t). \end{aligned} \tag{8}$$

The following lemma analyzes the asymptotic stability of the closed-loop dynamics in (8).

Lemma 1: Let Assumption 1 hold. The origin of (8) is locally asymptotically stable.

Proof: We choose the following Lyapunov function:

$$\mathscr{V}=\frac{1}{2}\tilde{\theta}^T\tilde{\theta}+\frac{1}{2}x_c^T x_c+W(\tilde{\theta}+\theta^*)-W(\theta^*)-\tilde{\theta}^T\nabla_{\tilde{\theta}+\theta^*}W(\theta^*) \tag{9}$$

where $\tilde{\theta}(t)=\left[\tilde{\theta}_1(t),\ldots,\tilde{\theta}_n(t)\right]^T$ and $x_c(t)=[x_{c_1}(t),\ldots,x_{c_n}(t)]^T$, and $W(\tilde{\theta})=-\mathbf{1}_n^T\Xi\cos(\mathbb{B}^T\tilde{\theta})$. First, $\mathscr{V}(\mathbf{0}_{2n})=0$. Moreover, it can be shown that $\mathscr{V}$ is positive around the origin. As W is strictly convex around the origin [16], $W(\tilde{\theta}+\theta^*)-W(\theta^*)-\tilde{\theta}^T\nabla_{\tilde{\theta}+\theta^*}$ is locally positive. As a result, $\mathscr{V}$ is positive around the origin. By direct calculation, the gradient of $\mathscr{V}$ is obtained as follows:

$$\nabla_{\tilde{\theta},x_c}\mathscr{V}=\begin{bmatrix} M_\theta^{-1}\tilde{\theta}+P_e(\tilde{\theta}) \\ x_c \end{bmatrix}, \tag{10}$$

where

$$P_e(\tilde{\theta})=\begin{bmatrix} \sum_{j\in\mathscr{N}_1} b_{1j}\left(\sin(\tilde{\theta}_{1j}(t)+\theta_{1j}^*)-\sin(\theta_{1j}^*)\right) \\ \cdots \\ \sum_{j\in\mathscr{N}_n} b_{nj}\left(\sin(\tilde{\theta}_{nj}(t)+\theta_{nj}^*)-\sin(\theta_{nj}^*)\right) \end{bmatrix}. \tag{11}$$

.

The time-derivative of $\mathscr{V}$ in (9) is obtained as follows:

$$\dot{\mathscr{V}}=-\frac{1}{2}\left(\tilde{\theta}^T r^{-1}\tilde{\theta}+P_e(\tilde{\theta})^T r^{-1}P_e(\tilde{\theta})\right)-x_c^T\eta x_c. \tag{12}$$

where $\eta=diag(\eta_1,\ldots,\eta_n)$ and $r=diag(r_1,\ldots,r_n)$. It is obvious that $\dot{\mathscr{V}}<0$. As a result, the origin of (8) is locally asymptotically stable. ■

Remark 1: The proposed resilient control scheme in (6) is distributed in the sense that the control design for IBR i requires the knowledge of the neighboring angles θ_j, $j\in\mathscr{N}_i$. However, (6) can be implemented in a fully decentralized way by measuring the active power $P_{e,i}(\theta)$ from PMUs.

IV. Input-Output Stability Analysis

It is assumed that the control input $u(t)$ is subject to a magnitude-bounded disturbance $\delta(t)=[\delta_1(t),\ldots,\delta_n(t)]^T\in\mathbb{R}^n$. Note that $\delta_j(t)=0$ if and only if the control input channel of the j-th IBR is not affected by any disturbance.

The main goal is to analyze the stability and resilience of the proposed angle controller in (6) against the magnitude-bounded disturbance. To this end, the closed-loop dynamics of (8) in the presence of the disturbance $\delta(t)$ can be represented as a Lur'e system, i.e., the interconnection of a linear time-invariant system and a nonlinear static state feedback, as follows:

$$\begin{aligned} \dot{x}(t) &= Ax(t)+B_\psi\psi(t)+B_\delta\delta(t), \\ y(t) &= C_y x(t), \\ z(t) &= C_z x(t), \end{aligned} \tag{13}$$

where

$$\psi(t)=\sin(z(t)+\phi^*)-\sin(\phi^*), \tag{14}$$

and $x(t)=\begin{bmatrix}\tilde{\theta}^T(t) & x_c^T(t)\end{bmatrix}^T\in\mathbb{R}^{2n}$ is the state vector, $y(t)=\tilde{\theta}(t)\in\mathbb{R}^n$ is the output vector, $z(t)=\mathbb{B}^T\tilde{\theta}(t)\in\mathbb{R}^m$ is the performance output, and $\phi^*=\mathbb{B}^T\theta^*$. The state space matrices are defined as follows:

$$\begin{aligned} &A=\begin{bmatrix} -\frac{1}{2}r^{-1} & -\beta \\ \beta & -\eta \end{bmatrix},\ B_\psi=\begin{bmatrix} -\frac{1}{2}r^{-1}M_\theta\mathbb{B}\Xi \\ \beta M_\theta\mathbb{B}\Xi \end{bmatrix}, \\ &B_\delta=\begin{bmatrix} \mathbf{I}_n \\ \mathbf{0}_{n\times n} \end{bmatrix},\ C_y=\begin{bmatrix}\mathbf{I}_n & \mathbf{0}_{n\times n}\end{bmatrix},\ C_z=\begin{bmatrix}\mathbb{B}^T & \mathbf{0}_{n\times n}\end{bmatrix}, \end{aligned} \tag{15}$$

where $\beta=\mathrm{diag}(\beta_1,\ldots,\beta_n)$ and $M_\theta=diag(m_{\theta_1},\ldots,m_{\theta_n})$.

It can be easily shown that A in (15) is a Hurwitz matrix. Furthermore, Under Assumption 1, the nonlinearity $\psi_i(t)$ in (13) is bounded, i.e., for each element $\psi_i(t)$,

$$|\ \psi_i(t)\ |\leq 1+\sin(\phi^*)$$

Moreover, $\left|\frac{\psi_i(t)}{z_i(t)}\right| \leq 1$ and $\gamma_{\psi,ii} = \sup_{z_i}\left|\frac{\psi_i(t)}{z_i(t)}\right| = \cos(\phi_i^*)$, where $\gamma_{\psi,ii}$ is the diagonal entry of a diagonal gain matrix γ_ψ. As $\gamma_{\psi,ii}$ is finite, the nonlinear term $\psi(t)$ is BIBO stable.

Let $G(s)$ be the transfer function matrix representing the linear dynamics between the inputs $\delta(t)$ and $\psi(t)$ and output $y(t)$ and $z(t)$ in the proposed Lur'e system in (13), represented as follows:

$$G(s) = \begin{bmatrix} G_{y,\delta}(s) & G_{y,\psi}(s) \\ G_{z,\delta}(s) & G_{z,\psi}(s) \end{bmatrix}, \tag{16}$$

where $G_{y,\delta}(s) = C_y(s\mathbf{I}_{2n}-A)^{-1}B_\delta$, $G_{y,\psi}(s) = C_y(s\mathbf{I}_{2n}-A)^{-1}B_\psi$, $G_{z,\delta}(s) = C_z(s\mathbf{I}_{2n}-A)^{-1}B_\delta$, and $G_{z,\psi}(s) = C_z(s\mathbf{I}_{2n}-A)^{-1}B_\psi$. By calculating the inverse of $s\mathbf{I}_{2n}-A$, one can obtain that

$$\begin{aligned} &G_{y,\delta}(s) = J(s), \\ &G_{y,\psi}(s) = -J(s)\left(\frac{1}{2}r^{-1} + \beta(s\mathbf{I}_n+\eta)^{-1}\beta\right)M_\theta\mathbb{B}\Xi, \\ &G_{z,\delta}(s) = \mathbb{B}^T J(s), \\ &G_{z,\psi}(s) = \mathbb{B}^T G_{y,\psi}(s), \end{aligned} \tag{17}$$

where

$$J(s) = \left((s\mathbf{I}_n + \frac{1}{2}r^{-1}) + \beta(s\mathbf{I}_n+\eta)^{-1}\beta\right)^{-1}. \tag{18}$$

The gain matrices of the stable transfer matrices $G_{z,\delta}(s)$, $G_{z,v}(s)$, $G_{y,\delta}(s)$, and $G_{y,v}(s)$ are respectively denoted by $\gamma_{z,\delta}$, $\gamma_{z,\psi}$, $\gamma_{y,\delta}$, and $\gamma_{z,\psi}$ in this paper and obtained using (1). In the following, we derive analytical solutions for the gain matrices as a function of control parameters and the physical parameters of the inverter-based microgrid.

A. Analytical Derivation of Gain Matrices

The transfer matrix $J(s)$ in (18) can be written as follows:

$$J(s) = \text{diag}\left(J_1(s),\ldots,J_n(s)\right), \tag{19}$$

where

$$J_i(s) = \frac{s+\eta_i}{(s+\frac{1}{4r_i}+\frac{\eta_i}{2})^2 + \beta_i^2 + \frac{1}{2r_i}\eta_i - (\frac{1}{4r_i}+\frac{\eta_i}{2})^2}, \tag{20}$$

for $i = 1,\ldots,n$. Hence, it can be shown that the impulse response of $J_i(s)$, denoted by $j_i(t)$, can be obtained by:

$$j_i(t) = \exp(a_i t)\left(\cos(b_i t) + c_i \sin(b_i t)\right) \tag{21}$$

where

$$\begin{aligned} a_i &= -(\frac{1}{4r_i}+\frac{\eta_i}{2}), \\ b_i &= \sqrt{\beta_i^2 + \frac{1}{2r_i}\eta_i - (\frac{1}{4r_i}+\frac{\eta_i}{2})^2}, \\ c_i &= \frac{-\frac{1}{4r_i}+\frac{\eta_i}{2}}{\sqrt{\beta_i^2 + \frac{1}{2r_i}\eta_i - (\frac{1}{4r_i}+\frac{\eta_i}{2})^2}}. \end{aligned} \tag{22}$$

By direct calculations and the use of summation formula of infinite geometric series, it can be shown that:

$$\gamma_{y,\delta_i} = \int_0^\infty |j_i(\tau)|d\tau \tag{23}$$

$$= -\frac{a_i}{a_i^2+b_i^2} + \frac{2a_i c_i \exp(\frac{\pi a_i}{2b_i}) + b_i c_i(1+\exp(\frac{\pi a_i}{b_i}))}{(1-\exp(\frac{\pi a_i}{b_i}))(a_i^2+b_i^2)}. \tag{24}$$

Due to the structure of the incidence matrix $\mathbb{B}$, the entities of $G_{z,\delta}(s) \in \mathbb{R}^{m\times n}$ are either 0 or $\pm J_i(s)$, $i \in \mathbb{V}$. Thus, it can be shown that

$$\gamma_{z,\delta}(s) = (\mathbb{B}^T)^{|.|}\gamma_{y,\delta},$$

where $(\mathbb{B}^T)^{|.|}$ indicates the element-wise absolute value of $\mathbb{B}^T$. Also, $G_{y,v}(s)$ can be rewritten as follows:

$$G_{y,\psi}(s) = -J_{y\psi}(s)M_\theta\mathbb{B}\Xi, \tag{25}$$

where

$$J_{y\psi}(s) = \text{diag}(J_{y\psi,1}(s),\ldots,J_{y\psi,n}(s)) \tag{26}$$

and

$$J_{y\psi,i}(s) = \frac{\frac{1}{2r_i}(s+\eta_i)+\beta_i^2}{(s+\frac{1}{4r_i}+\frac{\eta_i}{2})^2 + \beta_i^2 + \frac{1}{2r_i}\eta_i - (\frac{1}{4r_i}+\frac{\eta_i}{2})^2}, \tag{27}$$

for $i = 1,\ldots,n$. Denoting $j_{y\psi,i}(t)$ is the inverse Laplace transform of $J_{y\psi,i}(s)$, by direct calculation, it can be shown that

$$\begin{aligned} \int_0^\infty |j_{y\psi,i}(\tau)|d\tau = &-\frac{d_i a_i}{a_i^2+b_i^2} \\ &+ d_i f_i \frac{2a_i\exp(\frac{\pi a_i}{2b_i}) + b_i(1+\exp(\frac{\pi a_i}{b_i}))}{(1-\exp(\frac{\pi a_i}{b_i}))(a_i^2+b_i^2)}, \end{aligned} \tag{28}$$

where a_i and b_i are defined in (22) and

$$\begin{aligned} d_i &= \frac{1}{2r_i}, \\ f_i &= \frac{(\eta_i+a_i)+2r_i\beta_i^2}{b_i}. \end{aligned} \tag{29}$$

As a result, one can obtain that

$$\gamma_{y,\psi} = \text{diag}\left(\int_0^\infty |j_{y\psi,1}(\tau)|d\tau,\ldots,\int_0^\infty |j_{y\psi,n}(\tau)|d\tau\right)(\mathbb{B}\Xi)^{|.|}.$$

Furthermore, it can be shown that

$$\gamma_{z,\psi} = (\mathbb{B}^T)^{|.|}\gamma_{y,\psi}.$$

Remark 2: For the conventional droop angle control in (5), one can obtain that

$$\begin{aligned} &\gamma_{y,\delta} = \text{diag}\left(2r_1,\ldots,2r_n\right), \\ &\gamma_{y,\psi} = M_\theta(\mathbb{B}\Xi)^{|.|}, \\ &\gamma_{z,\delta} = (\mathbb{B}^T)^{|.|}\,\text{diag}\left(2r_1,\ldots,2r_n\right), \\ &\gamma_{z,\psi} = (\mathbb{B}^T)^{|.|}M_\theta(\mathbb{B}\Xi)^{|.|}. \end{aligned} \tag{30}$$

B. Design of Control Parameters

We can further relax the choice of the control parameters r_i, η_i, and β_i by simply requiring the following constraint on the control design parameters:

$$\beta_i^2 + \frac{1}{2r_i}\eta_i = (1+e^{-\pi\mu})\left(\frac{1}{4r_i}+\frac{\eta_i}{2}\right)^2, \tag{31}$$

where $\mu \approx -0.47454$ is a negative constant, and $\mu = -\frac{2}{\pi}\mathrm{w}_0(\frac{2}{\pi}) < 0$ with $\mathrm{w}_0(\cdot)$ the Lambert W-function, namely μ is the unique solution of

$$\exp(\frac{\pi\mu}{2}) + \mu = 0. \tag{32}$$

If (31) holds, we can show that

$$a_i = -b_i \exp(\frac{\pi\mu}{2}) = -b_i \exp(\frac{\pi a_i}{2b_i}), \tag{33}$$

holds for all a_i and b_i. Taking (33) into consideration, we simplify the expressions (23) and (28) as follows:

$$\gamma_{y,\delta_i}(\beta_i) = \frac{-a_i + b_i c_i}{a_i^2 + b_i^2} = \frac{\eta_i}{\beta_i^2 + \frac{1}{2r_i}\eta_i} \tag{34}$$

$$\int_0^\infty |j_{y\psi,i}(\tau)| d\tau = \frac{-d_i a_i + f_i b_i}{a_i^2 + b_i^2} = \frac{1}{2r_i}\frac{\eta_i + 2r_i\beta_i^2}{\beta_i^2 + \frac{1}{2r_i}\eta_i} \tag{35}$$

$$= 1. \tag{36}$$

Let η_i and r_i be chosen to satisfy (31). Then, increasing β_i leads to smaller gains. Consequently, the gain matrices are obtained as follows:

$$\begin{aligned}
&\gamma_{y,\delta} = \mathrm{diag}\left(\frac{\eta_1}{\beta_1^2+\frac{1}{2r_1}\eta_1}, \ldots, \frac{\eta_n}{\beta_n^2+\frac{1}{2r_n}\eta_n}\right),\\
&\gamma_{y,\psi} = M_\theta(\mathbb{B}\Xi)^{|\cdot|},\\
&\gamma_{z,\delta} = (\mathbb{B}^T)^{|\cdot|}\,\mathrm{diag}\left(\frac{\eta_1}{\beta_1^2+\frac{1}{2r_1}\eta_1}, \ldots, \frac{\eta_n}{\beta_n^2+\frac{1}{2r_n}\eta_n}\right),\\
&\gamma_{z,\psi} = (\mathbb{B}^T)^{|\cdot|} M_\theta(\mathbb{B}\Xi)^{|\cdot|}.
\end{aligned} \tag{37}$$

C. Bounded-Input Bounded-Output Stability

The following lemma presents sufficient conditions for the Bounded-Input Bounded-Output (BIBO) stability of the Lur'e system in (13).

Lemma 2: The Lur'e system in (13) is BIBO stable if $\rho(\gamma_{z,\psi}\gamma_\psi) < 1$.

Proof: If $\rho(\gamma_{z,\psi}\gamma_\psi) < 1$, $\mathbf{I}_m - \gamma_{z,\psi}\gamma_\psi$ is inverse-positive. Thus, using norm properties, one can show that

$$\|y\|_{\mathscr{L}_\infty} \le \left(\gamma_{y,\delta} + \gamma_{y,\psi}\gamma_\psi(\mathbf{I}_m - \gamma_{z,\psi}\gamma_\psi)^{-1}\gamma_{z,\delta}\right)\|\delta\|_{\mathscr{L}_\infty}. \tag{38}$$

As the gain matrices $\gamma_{y,\delta}$, $\gamma_{y,\psi}$, $\gamma_{z,\delta}$, $\gamma_{z,\psi}$, and the nonlinearity gain γ_ψ are finite, for a bounded $\|\delta\|_{\mathscr{L}_\infty}$, $\|y\|_{\mathscr{L}_\infty}$ is bounded. This implies the BIBO stability of the Lur'e system in (13). ■

The BIBO stability conditions in Lemma 2 depend on the microgrid topology and droop gains and are independent of the control parameters r, η, and β. However, in the following, we show that these parameters impact the resilience of the IBR-based system and should be appropriately designed.

D. Characterization of Resilience Metrics

The transient and steady-state performance specification introduces constraints on the difference between the phase angles of adjacent buses θ_{ij}, $\forall\ i,j \in \mathbb{V}$, to ensure that the inverter-based system remains synchronized during the transient and steady-state. These operational constraints are mathematically formulated as follows:

1) Transient-state frequency bounds: $\|y\|_{\mathscr{L}_\infty} \le \bar{y}$ in which $\bar{y} \in \mathbb{R}^n$ is the maximum phase angle deviation.
2) Transient-state power flow bounds: $\|z\|_{\mathscr{L}_\infty} \le \bar{z}$, where $\bar{z} \in \mathbb{R}^m$.

Note that the maximum phase angle difference in a typical power system is in the order of $\pi/18$ to $\pi/9$ rad [17].

Let us assume that $\bar{\delta} \in \mathbb{R}^n$ is a bound on the element-wise $\mathscr{L}_\infty$ norm of $\delta(t)$, i.e., $\|\delta\|_{\mathscr{L}_\infty} \le \bar{\delta}$. The following lemma assesses if the inverter-based microgrid satisfies the above-mentioned operational constraints in the presence of the disturbance $\delta(t)$ with $\|\delta\|_{\mathscr{L}_\infty} \le \bar{\delta}$.

Lemma 3: If there exist $\bar{\delta} \in \mathbb{R}^n$ and $\bar{z} \in \mathbb{R}^m$ so that the following conditions are satisfied:

$$(\mathbb{B}^T)^{|\cdot|}\left(\gamma_{y,\delta}\bar{\delta} + \gamma_{y,\psi}\cos(\phi^*)\bar{z}\right) < \bar{z}, \tag{39a}$$

$$\gamma_{y,\delta}\bar{\delta} + \gamma_{y,\psi}\cos(\phi^*)\bar{z} \le \bar{y}, \tag{39b}$$

the Lur'e system in (13) is constrained input constrained output (CICO) stable and $\|y\|_{\mathscr{L}_\infty} \le \bar{y}$ and $\|z\|_{\mathscr{L}_\infty} \le \bar{z}$.

Proof: Using norm properties, one can show that

$$\begin{aligned}
\|y\|_{\mathscr{L}_\infty} &\le \gamma_{y,\delta}\|\delta\|_{\mathscr{L}_\infty} + \gamma_{y,\psi}\gamma_\psi\|z\|_{\mathscr{L}_\infty} \le \gamma_{y,\delta}\bar{\delta} + \gamma_{y,\psi}\gamma_\psi\bar{z},\\
\|z\|_{\mathscr{L}_\infty} &\le \gamma_{z,\delta}\|\delta\|_{\mathscr{L}_\infty} + \gamma_{z,\psi}\gamma_\psi\|z\|_{\mathscr{L}_\infty} \le \gamma_{z,\delta}\bar{\delta} + \gamma_{z,\psi}\gamma_\psi\bar{z}.
\end{aligned} \tag{40}$$

Considering $\gamma_\psi = \cos(\phi^*)$, $\gamma_{z,\delta} = (\mathbb{B}^T)^{|\cdot|}\gamma_{y,\delta}$ and $\gamma_{z,\psi} = (\mathbb{B}^T)^{|\cdot|}\gamma_{y,\psi}$ (see (37)), from the above inequalities and (39), one can obtain that $\|y\|_{\mathscr{L}_\infty} \le \bar{y}$ and $\|z\|_{\mathscr{L}_\infty} \le \bar{z}$. ■

The inequality constraints given in (39) characterize the tolerable disturbances for the transient-state safety in an inverter-based microgrid. In the following, the impact of β_i on the gain matrices will be discussed.

According to (37), by increasing the value of β_i, the entities of $\gamma_{y,\delta}$ and $\gamma_{z,\delta}$ decreases while the entities of $\gamma_{y,\psi}$ and $\gamma_{z,\psi}$ remain unchanged. According to (39), this indicates that for the pre-defined bound $\bar{y}$, the inverter-based microgrid with the proposed control scheme in (6) can tolerate a larger disturbance (a larger (element-wise) value of $\bar{\delta}$) with a bound of $\bar{z}$. Consequently, it highlights the resilience property of the proposed angle droop control in (6) compared to the conventional angle droop control in (5).

Remark 3: The constraints in (39) are in terms of linear matrix inequalities (LMIs) with respect to $\bar{\delta}$ and $\bar{z}$. These constraints can be used for estimating the upper bound on the disturbance magnitude $\bar{\delta}$ (the admissible disturbance that the IBR-based power system can tolerate) while satisfying the operational constraints in inverter-based microgrids.

V. Simulation Results

We consider a microgrid composed of three IBRs with a loop topology, controlled using cascaded voltage control loops. The initial reference angle vector of the IBRs (in rad)

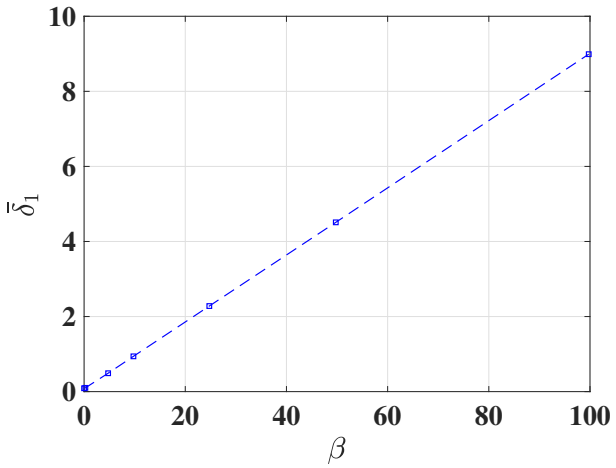

Fig. 1. Upper bound on the disturbance magnitude versus β_i.

is set at $\theta_0^* = [0.951\ 0.92\ 0.967]^T$ that satisfies Assumption 1. The microgrid operates at the rated angular frequency $\omega^* = 2\pi \times 50\ rad/s$.

The effectiveness and performance of the proposed resilient angle control scheme in (6) in terms of frequency synchronization and angle stabilization is demonstrated via time-domain simulations under nominal (normal) conditions and disturbances. In the proposed angle controller, the control parameters are set as $r = \mathbf{I}_3$, $\eta = 20\mathbf{I}_3$, $\beta_1 = \beta_2 = \beta_3$.

For the microgrid system, $\rho(\gamma_{z,\psi}\cos(\phi^*)) = 0.1521$, which is smaller than one. Hence, the condition for the BIBO stability stated in Lemma 2 is satisfied.

In the next stage, we assess the impact of β on the resilience of the proposed control law in (6) with respect to a bounded disturbance $\delta_1(t)$ affecting IBR 1. To this end, we determine the maximum admissible disturbance $\bar{\delta}_1$ for a given $\bar{y} = [0.2\ \ 0.24\ \ 0.19]^T$ by solving the convex optimization problem subject to the set of LMIs given in (39). The optimization problem is solved by MOSEK [18] as a solver and YALMIP [19] as an interface.

Fig. 1 depicts the value of $\bar{\delta}_1$ in per unit (p.u.) as a function of β_i. The maximum phase difference deviation $\bar{z}$ for all values of β_i reported in Fig. 1 is $\bar{z} = [0.21\ \ 0.21]^T$. As one can see from Fig. 1, for a fixed $\bar{z}$ and $\bar{y}$, the proposed control law in (6) with a higher β can allow a large disturbance magnitude. Note that when $\beta = \mathbf{0}_{3\times 3}$ (i.e., the conventional angle droop control in (5)), $\bar{\delta}_1 = 0.0895$ p.u. The results highlight the resilience property of the proposed angle control approach in (6).

VI. Conclusion

This paper deals with the resilience-enhancing problem in angle control of inverter-interfaced microgrid in the presence of magnitude-bounded disturbance. The paper develops an angle control strategy with built-in resilience solutions. To this end, we propose a resilience assessment framework that incorporate the operational constraints in frequency synchronization and phase angle differences of microgrids. The framework will facilitate a quantitative measure to show the effectiveness of proposed resilient angle control approach. Rigorous input-output stability conditions are proposed. Simulation results demonstrate the effectiveness and resilience performance of the proposed angle control strategy for inverter-based microgrids. The future work includes the extension of this work to the detailed model of inverter-interfaced microgrids.

References

[1] "IEC TS 62898-1 Technical Specification: Microgrids –Part 1: Guidelines for microgrid projects planning and specification," British Standards Institute, 2017.

[2] F. Milano, F. Dörfler, G. Hug, D. J. Hill, and G. Verbic, "Foundations and challenges of low-inertia systems," in *Power Systems Computation Conference (PSCC)*, Dublin, Irland, June 2018, pp. 1–25.

[3] M. S. Sadabadi, "A resilient-by-design distributed control framework for cyber-physical DC microgrids," *IEEE Transactions on Control Systems Technology*, vol. 32, no. 2, pp. 625–636, 2024.

[4] M. S. Sadabadi, S. Sahoo, and F. Blaabjerg, "A fully resilient cyber-secure synchronization strategy for AC microgrids," *IEEE Transactions on Power Electronics*, vol. 36, no. 12, pp. 13 372–13 378, 2021.

[5] R. Yan, N.-A. Masood, T. Kumar Saha, F. Bai, and H. Gu, "The anatomy of the 2016 South Australia blackout: A catastrophic event in a high renewable network," *IEEE Transactions on Power Systems*, vol. 33, no. 5, pp. 5374–5388, 2018.

[6] "Black system South Australia 28 september 2016 – integrated final report," AEMO, Melbourne, VIC, Australia, 2017.

[7] R. Majumder, G. Ledwich, A. Ghosh, S. Chakrabarti, and F. Zare, "Droop control of converter-interfaced microsources in rural distributed generation," *IEEE Transactions on Power Delivery*, vol. 25, no. 4, pp. 2768–2778, 2010.

[8] R. R. Kolluri, I. Mareels, T. Alpcan, M. Brazil, J. de Hoog, and D. A. Thomas, "Power sharing in angle droop controlled microgrids," *IEEE Transactions on Power Systems*, vol. 32, no. 6, pp. 4743–4751, 2017.

[9] R. Majumder, A. Ghosh, G. Ledwich, and F. Zare, "Angle droop versus frequency droop in a voltage source converter based autonomous microgrid," in *2009 IEEE Power Energy Society General Meeting*, 2009, pp. 1–8.

[10] R. Majumder, B. Chaudhuri, A. Ghosh, R. Majumder, G. Ledwich, and F. Zare, "Improvement of stability and load sharing in an autonomous microgrid using supplementary droop control loop," *IEEE Transactions on Power Systems*, vol. 25, no. 2, pp. 796–808, 2010.

[11] T. Jouini, A. Rantzer, and E. Tegling, "Inverse optimal control for angle stabilization in converter-based generation," in *2022 American Control Conference (ACC)*, 2022, pp. 4945–4950.

[12] D. Lee, L. Aolaritei, T. L. Vu, and K. Turitsyn, "Robustness against disturbances in power systems under frequency constraints," *IEEE Transactions on Control of Network Systems*, vol. 6, no. 3, pp. 971–979, 2019.

[13] J. H. Kim, Y. W. Choi, and T. Hagiwara, "Computing the L_∞-induced norm of LTI systems: Generalization of piecewise quadratic and cubic approximations," *IEEE Access*, vol. 8, pp. 139 868–139 880, 2020.

[14] J. H. Kim and T. Hagiwara, "Computing the L_∞-induced norm of LTI systems," in *53rd IEEE Conference on Decision and Control*, 2014, pp. 2404–2409.

[15] J. E. Peris, "A new characterization of inverse-positive matrices," *LINEAR ALGEBRA AND ITS APPLICATIONS*, pp. 45–58, 1991.

[16] P. Monshizadeh, C. De Persis, T. Stegink, N. Monshizadeh, and A. van der Schaft, "Stability and frequency regulation of inverters with capacitive inertia," in *2017 IEEE 56th Annual Conference on Decision and Control (CDC)*, 2017, pp. 5696–5701.

[17] P. Bonanomi, "Phase angle measurements with synchronized clocks-principle and applications," *IEEE Transactions on Power Apparatus and Systems*, vol. PAS-100, no. 12, pp. 5036–5043, 1981.

[18] M. ApS, *The MOSEK optimization toolbox for MATLAB manual. Version 9.0.*, 2019. [Online]. Available: http://docs.mosek.com/9.0/toolbox/index.html

[19] J. Löfberg, "YALMIP : A toolbox for modeling and optimization in MATLAB," in *In Proceedings of the CACSD Conference*, Taipei, Taiwan, 2004.